

A study of the neglected Galactic H II region NGC 2579 and its companion ESO 370-9

M. V. F. Copetti¹, V. A. Oliveira¹, R. Riffel², H. O. Castañeda³, and D. Sanmartim¹

¹ Laboratório de Análise Numérica e Astrofísica, Departamento de Matemática, e Programa de Pós-Graduação em Física, Universidade Federal de Santa Maria, 97119-900 Santa Maria, RS, Brazil.

² Departamento de Astronomia, Universidade Federal do Rio Grande do Sul. Av. Bento Gonçalves 9500, Porto Alegre, RS, Brazil

³ Instituto de Astrofísica de Canarias, La Laguna, Tenerife, E-38200 Canary Islands, Spain

Received 15 May 2007 / Accepted 15 June 2007

ABSTRACT

Context. The Galactic H II region NGC 2579 has stayed undeservedly unexplored due to identification problems which persisted until recently. Both NGC 2579 and its companion ESO 370-9 have been misclassified as planetary or reflection nebula, confused with each other and with other objects. Due to its high surface brightness, high excitation, angular size of few arcminutes and relatively low interstellar extinction, NGC 2579 is an ideal object for investigations in the optical range. Located in the outer Galaxy, NGC 2579 is an excellent object for studying the Galactic chemical abundance gradients.

Aims. To present the first comprehensive observational study on the nebular and stellar properties of NGC 2579 and ESO 370-9, including the determination of electron temperature, density structure, chemical composition, kinematics, distance, and the identification and spectral classification of the ionizing stars, and to discuss the nature of ESO 370-9.

Methods. Long slit spectrophotometric data in the optical range were used to derive the nebular electron temperature, density and chemical abundances and for the spectral classification of the ionizing star candidates. H α and *UBV* CCD photometry was carried out to derive stellar distances from spectroscopic parallax and to measure the ionizing photon flux.

Results. The chemical abundances of He, N, O, Ne, S, Cl, and Ar were obtained. Maps of electron density and radial velocity with a spatial resolution of 5'' \times 5'' were composed from long slit spectra taken at different declinations. Three O stars classified as O5 V, O6.5 V, and O8 V were found responsible for the ionization of NGC 2579, while ESO 370-9 is ionized by a single O8.5 V star. The estimated mass of ionized gas of $\approx 25 M_{\odot}$ indicates that ESO 370-9 is not a planetary nebula, but a small H II region. A photometric distance of 7.6 ± 0.9 kpc and a kinematic distance of 7.4 ± 1.4 kpc were obtained for both objects. At the galactocentric distance of 12.8 ± 0.7 kpc, NGC 2579 is one of the most distant Galactic H II regions for which direct abundance determinations have been accomplished.

Key words. ISM: H II regions – ISM: planetary nebulae

1. Introduction

Due to observational difficulties, the knowledge acquisition in many research areas of astrophysics has still relied largely on data obtained from a small group of characteristic objects. This is certainly the case of the optical studies of Galactic H II regions. In this field, the Orion Nebula is by far the most studied object. In fact, the number of papers on this object is comparable to the total number of optical studies of all other Galactic H II regions. Even the standard procedure of measuring the electron temperature in Galactic H II regions from optical emission line ratios, such as [O III] ($\lambda 4959 + \lambda 5007$)/ $\lambda 4363$ and [N II] ($\lambda 6548 + \lambda 6584$)/ $\lambda 5755$, until now could only be accomplished in a small sample of a dozen or so objects. So, the addition of new members to the selected list of well studied (or easy to observe) objects is welcome, especially because the H II regions are good tracers of the chemical abundance variation across the disk of the Galaxy.

The Galactic H II region NGC 2579 (centred at $\alpha = 08:20:54.8$, $\delta = -36:12:59.9$, J2000), because of its high surface brightness, angular size of few arcminutes and relatively low interstellar extinction, is an ideal object for investigations in the optical range, but stays undeservedly unexplored due to

identification problems which persisted until recently. Despite its description as a “double star in a pretty small nebula among 70 stars” and sufficiently precise coordinates in the New General catalogue (Dreyer, 1888), NGC 2579 has been confused with other nearby (and not so nearby) objects, as the open clusters NGC 2580 and AH03 J0822-36 (Archinal & Hynes, 2003), which show no clear signs of nebulosity. The only *UBV* photometric study found in the literature of the stars claimed to be in NGC 2579, by Lindoff (1968), is in fact on stars pertaining to the cluster AH03 J0822-36, which lies approximately 20' to the Southeast of the supposed object. NGC 2579 is sometimes incorrectly associated with the nebula RCW 20. Correct identifications of NGC 2579 are with Gum 11 (Gum, 1955) and BBW 138 (Brand et al., 1986).

NGC 2579 has been misclassified as a reflection nebula (e.g., in the SIMBAD database) because of the association with the objects VdBH 13a, VdBH 13b, and VdBH 13c wrongly considered of this kind. These objects are in fact stars towards NGC 2579 listed in the catalogue of “southern stars embedded in nebulosity” by van den Bergh & Herbst (1975), which was a result of a survey of southern reflection nebulae conducted by these authors. However, not all of the stars in the catalogue are really associated with reflection nebulae. As another example of the confusion involving the identification of NGC 2579, these au-

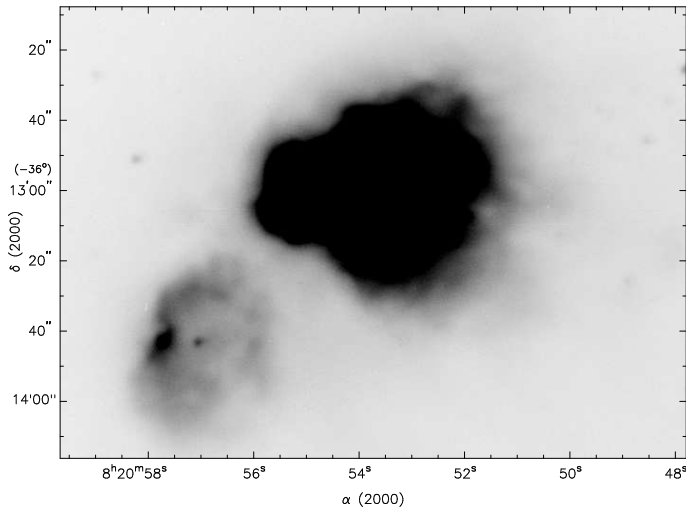


Fig. 1. $H\alpha$ image of NGC 2579 (brighter nebula) and ESO 370-9

thors mistakenly associated VdBH 13a, b, c with NGC 2580, an open cluster more than 6 degrees away from the observed position.

NGC 2579 was “rediscovered” as the emission nebula Ns 238 in the objective prism survey by Nordstrom (1975) and classified as a probable planetary nebula. It is identified as PN G254.6+00.2 in the Strasbourg-ESO catalogue of Galactic planetary nebulae (Acker et al., 1992). However, doubts about the planetary nebula nature of this object were raised (Kimeswenger, 2001), based on the morphology, IRAS colors and total far infrared flux.

To complicate the matter, NGC 2579 has a very close companion, the object ESO 370-9, a small ($\sim 1'$) roughly elliptical ringed nebula with a star in the middle ($\alpha = 08:20:56.75$, $\delta = -36:13:46.9$, J2000). It was discovered and classified as a planetary nebula candidate by Lauberts et al. (1981, the original identification was 370-PN?09). In the SIMBAD database ESO 370-9 is classified as a reflection nebula, because of its association with VdBH 13c, which is its central star. It is also confused with the misclassified planetary nebula PN G254.6+00.2 (in fact with H II region NGC 2579).

In this paper, we present the first comprehensive optical study on the nebular and stellar properties of the Galactic H II region NGC 2579 and its companion ESO 370-9, including the determination of electron temperature, density structure, chemical composition, kinematics, distance, and the identification and spectral classification of its ionizing stars. We also discuss the nature of ESO 370-9. In Fig. 1 we present an $H\alpha$ image of the area of NGC 2579 and ESO 370-9, which shows that these two nebula are distinct objects.

2. Observations and data reductions

2.1. Spectroscopy

Long slit spectrophotometric observations were carried out with the Boller & Chivens spectrograph attached to the 1.52 m telescope at the European Southern Observatory (ESO), La Silla, Chile, and with the Cassegrain spectrograph attached to the 1.6 m telescope at Observatório do Pico dos Dias (OPD), Brasópolis, Brazil. At ESO we used a Loral CCD of 2688×512 pixels and a grid of 1200 grooves mm^{-1} , resulting in a spatial scale of $1.64'' \text{pxl}^{-1}$ (after the rebinning of each two contiguous CCD rows to increase the signal-to-noise ratio), a spectral dispersion

Table 1. Journal of spectroscopic observations

$\Delta\delta$	Obs./Tel.	Date	Wavelength range (\AA)	Exposure (s)
0''	ESO 1.52 m	2002 Dec 30	3300–5100	3×1200
	ESO 1.52 m	2002 Dec 31	4630–6750	3×1200
8'' N	ESO 1.52 m	2002 Dec 30	3300–5100	1×1200
	ESO 1.52 m	2003 Jan 01	3300–5100	2×1200
	ESO 1.52 m	2002 Dec 31	4630–6750	2×600
7'' S	ESO 1.52 m	2003 Jan 01	3300–5100	3×1200
	ESO 1.52 m	2002 Dec 31	4630–6750	3×600
44'' S	OPD 1.60 m	2006 Apr 20	4030–4990	3×1200
	OPD 1.60 m	2006 Apr 24	4000–7750	3×1200
0''	OPD 1.60 m	2004 Apr 22	6000–7000	2×1200
5'' N	OPD 1.60 m	2004 Nov 08	6000–7000	1×600
10'' N	OPD 1.60 m	2004 Apr 22	6000–7000	1×1200
15'' N	OPD 1.60 m	2004 Apr 22	6000–7000	2×1200
20'' N	OPD 1.60 m	2004 Nov 08	6000–7000	2×600
25'' N	OPD 1.60 m	2004 Apr 22	6000–7000	1×1200
	OPD 1.60 m	2004 Nov 08	6000–7000	1×1200
30'' N	OPD 1.60 m	2004 Apr 22	6000–7000	1×1200
	OPD 1.60 m	2004 Nov 08	6000–7000	1×1200
5'' S	OPD 1.60 m	2004 Apr 23	6000–7000	1×1200
10'' S	OPD 1.60 m	2004 Apr 23	6000–7000	1×1200
15'' S	OPD 1.60 m	2004 Apr 23	6000–7000	1×1200
20'' S	OPD 1.60 m	2004 Apr 23	6000–7000	1×1200
25'' S	OPD 1.60 m	2004 Apr 23	6000–7000	1×1200
30'' S	OPD 1.60 m	2004 Apr 23	6000–7000	1×1200
35'' S	OPD 1.60 m	2004 Apr 23	6000–7000	1×1200
40'' S	OPD 1.60 m	2004 Apr 23	6000–7000	1×1200

of 1.0 \AA pxl^{-1} , and a resolution of 2.9 \AA . At the OPD we used a SITe CCD of 2048×2048 pixels, resulting in a spatial scale of $0.56'' \text{pxl}^{-1}$, and two different grids. Spectra in the range of 4000 to 7750 \AA , with dispersion of 2.4 \AA pxl^{-1} and resolution of about 8 \AA , were obtained with a grid of 300 mm^{-1} , while a grid of 1200 grooves mm^{-1} was used to obtain spectra in the 4030–4990 \AA and 6000–7000 \AA ranges, with dispersion of 0.5 \AA pxl^{-1} and mean resolution of 2.7 \AA . Table 1 presents the journal of observations. The columns are the declination offset $\Delta\delta$ of the slit relative to reference star DENIS J082054.8-361258 ($\alpha = 08:20:54.86$, $\delta = -36:12:58.9$, epoch J2000), the observatory and telescope used, the spectral range, and the number and time of the exposures.

The observation routine followed usual procedures. Dome flat-field exposures were taken at the beginning and at the end of each night. About 30 bias frames were made per night. Spectrophotometric standard stars were observed for flux calibration. Spectra of a He–Ar–Ne lamp were taken before and after each object exposure for wavelength calibration. Exposure times were limited to 20 minutes to reduce the effects of cosmic rays.

The slits used had entrances on the plane of sky of $2'' \times 250''$ for the observations at ESO and $1.5'' \times 320''$ for the observations at OPD, and they were aligned along the east-west direction. For the identification and spectral classification of the ionizing star (see Sect. 5), in some of the observations, the slit was set passing through some plausible ionizing star candidate. Spectra of the four brightest stars on the image of NGC 2579 and of the central star in ESO 370-9 were obtained with slit declination corresponding to $\Delta\delta = 0''$, 8'' N, 7'' S, and 44'' S. These spectra cover most of the optical range and were also used for nebular abundance determinations (see Sect. 3). In the other observations,

the slit was positioned at 15 different and equally spaced declinations separated by $5''$. The 2D spectra obtained in the range 6000–7000 Å, sampling the whole nebula NGC 2579 and part of ESO 370-9, were used to produce maps of electron density and radial velocity (see Sect. 4).

The data reduction (bias correction, flat-fielding, cosmic rays cleaning, wavelength and flux calibration, 1D spectrum extraction) followed standard procedures and was made with the IRAF software. From the combined spectra acquired at $\Delta\delta = 0''$, $8''$ N, $7''$ S, and $44''$ S., five 1D stellar spectra and four nebular spectra integrated along the slit were obtained. Due to the great and irregular surface brightness of the nebula, the background subtraction for the stellar spectra was difficult and many attempts had to be made to eliminate the contamination of the nebular emission lines. From each of the 2D spectra obtained at equally spaced declinations, we extracted a series of 1D spectra from contiguous sectors of $5''$ of length along the slit axis (east-west direction). To secure 1D spectra from sectors along the same north-south strips, we first had to define a fiducial position on the slit axis, by measuring in the 2D spectrum spatial profiles the position of the detected star and comparing them with coordinates obtained from direct images of the region. In this way, we extracted 750 1D spectra from individual sectors of size $5'' \times 1.5''$ centred on a grid of 50×15 equally spaced points, sampling the nebula with a spatial resolution of $5'' \times 5''$.

The emission line fluxes were obtained by Gaussian fitting of the line profile and by direct integration of the flux over a linear local continuum defined by eye carried out with the *splot* routine of the IRAF package. We estimated the error associated with the line fluxes by $\sigma^2 = \sigma_{\text{cont}}^2 + \sigma_{\text{line}}^2 + \sigma_{\text{cal}}^2 + \sigma_{\text{meth}}^2$, where σ_{cont} is the error due to the continuum baseline determination, σ_{line} is the Poisson error of the emission line, σ_{cal} is the error due to the flux calibration (measured as the standard deviation of the residual of the fitting of the standard star calibration curves), and σ_{meth} is the error due to the method of integration of the line flux. All the line intensities were normalized to H β and corrected for the effect of the interstellar extinction by comparing the observed ratios H α /H β , H γ /H β and H δ /H β with the theoretical ones calculated by Storey & Hummer (1995) for an electron temperature of 10 000 K and a density of 100 cm^{-3} . The Galactic reddening function of Kaler (1976) was used. In some positions, significantly different values for the logarithmic extinction coefficient $c(\text{H}\beta)$ were obtained from the blue and red spectra. To mitigate possible systematic errors in the flux calibration which could be responsible for these differences, the intensities of the lines with wavelength larger than that of H β were corrected with $c(\text{H}\beta)$ calculated from the H α /H β ratio and for the other lines we used the mean value from the H γ /H β and H δ /H β ratios. Table 4 lists the observed and reddening-corrected emission line intensities relative to H β and the logarithmic extinction coefficient $c(\text{H}\beta)$ from the integrated spectra obtained for NGC 2579 at offset declinations $\Delta\delta = 0''$, $8''$ N, $7''$ S (hereafter labelled A, B, and C, respectively), from the sum of these three spectra (labelled ABC), and for ESO 370-9 from the spectrum obtained at $\Delta\delta = 44''$ S.

2.2. *UBV* photometry

Direct images in the *UBV* filters were obtained with the 1.5 m telescope at the San Pedro Mártir Observatory (SPM), B.C., Mexico and with the 0.6 m Boller & Chivens telescope at the Observatório do Pico dos Dias (OPD), Brasópolis, Brazil, in March 2000 and April 2005, respectively. To avoid saturation of the brightest stars, multiple exposures of different times were

Table 2. Journal of photometric observations

Filter	Obs./Tel.	Date	Exposure (s)
U	SPM 1.5 m	2000 Mar 10	3×300
	SPM 1.5 m	2000 Mar 14	1×300
B	SPM 1.5 m	2000 Mar 10	$2 \times 300 + 1 \times 100$
	SPM 1.5 m	2000 Mar 14	$1 \times 300 + 1 \times 200$
	OPD 0.6 m	2005 Apr 10	$5 \times 240 + 5 \times 120$
V	SPM 1.5 m	2000 Mar 10	$1 \times 60 + 1 \times 30 + 1 \times 20$
	SPM 1.5 m	2000 Mar 14	1×30
	OPD 0.6 m	2005 Apr 10	$5 \times 45 + 7 \times 35 + 5 \times 25$
H α	SPM 1.5 m	2000 Mar 15	5×300
Cont.	SPM 1.5 m	2000 Mar 15	4×60

Table 3. Interference filters

Filter	λ_c (Å)	Peak trans.	FWHM (Å)	Effec. width (Å)
H α	6563	66.4%	9.8	5.4
Cont.	6450	95.0%	127	114

taken in each filter. Several dome flat-field and bias exposures were taken at the beginning and at the end of each night. The *UBV* Landolt (1992) standard star fields SA 99-447/438, SA 106-700 were observed at the OPD and PG 0918+029, PG 1323-086 and Feige 34 at SPM. About 40 secondary standard stars measured by Galadí-Enríquez et al. (2000) were found in these fields. The journal of the photometric observations is presented in Table 2. The seeing ranged from $1.5''$ to $2.5''$ in different nights.

The reduction followed the standard procedure for stellar CCD photometry in a relatively crowded field and was performed with the IRAF/Daophot package.

2.3. *H* α photometry

To measure the H α flux of the nebulae we also obtained CCD images in narrow-band interference filters in H α and near continuum with the 1.5 m telescope at the San Pedro Mártir Observatory. The log of observations is in Table 2. The spectrophotometric standard star Feige 34 was observed for flux calibration. Details of the filters, including the central wavelength λ_c , effective bandwidth, peak transmission, and full width at half maximum (FWHM), are presented in Table 3. After the standard CCD data reduction, the brightest stars were eliminated from the images by interpolation of nearby data points and the total counts in each filter within a polygonal area encompassing the nebulae were obtained. After this we followed a procedure similar to that described by Copetti & Dottori (1989) to calculate the H α flux from the counts, taking into account the small but not insignificant contribution of the nebular emission lines [S III] λ 6312, [N II] λ 6583 and even H α to the counts in the continuum filter. We obtained H α fluxes (in $\text{erg cm}^{-2} \text{ s}^{-1}$) of $\log F(\text{H}\alpha) = -9.68$ for NGC 2579 and $\log F(\text{H}\alpha) = -10.58$ for ESO 370-9.

3. Chemical abundance analysis

The emission line intensities listed in Table 4 were used for chemical abundance analysis of the nebulae.

3.1. Electron densities and temperatures

The electron temperature estimates referred as $T_e(\text{O III})$ and $T_e(\text{N II})$ were derived from the $[\text{O III}](\lambda 4959 + \lambda 5007)/\lambda 4363$ and $[\text{N II}](\lambda 6548 + \lambda 6583)/\lambda 5755$ line intensity ratios and the electron density estimates $N_e(\text{S II})$ and $N_e(\text{Cl III})$ from the $[\text{S II}]\lambda 6716/\lambda 6731$ and $[\text{Cl III}]\lambda 5517/\lambda 5537$ ratios, respectively. These electron temperatures and densities were obtained by solving numerically the equilibrium equations for an n -level atom ($5 \leq n \leq 9$) using the *temden* routine of the *nebular* package of the *STSDAS/IRAF*, using the same atomic parameters as in Krabbe & Copetti (2005). Table 5 lists the electron densities and temperatures obtained. For $N_e(\text{Cl III})$ only upper limits were presented because the error interval for the $[\text{Cl III}]\lambda 5517/\lambda 5537$ ratio extends beyond the low density limit.

3.2. Abundance determination

We have derived ionic and total abundances of He, N, O, Ne, S, Cl, and Ar. Although we have detected some recombination lines of heavy elements, their intensities are too uncertain to be used in the abundance analysis. We thus relied only upon the collisionally excited lines to calculate abundances of metals. Based on the similarity of the ionization potentials, we adopted for NGC 2579 the electron temperature $T_e(\text{N II})$ for the N^+ , O^+ , and S^+ ionic zones, and $T_e(\text{O III})$ for O^{++} , Ne^{++} , S^{++} and Cl^{++} . For ESO 370-9, because we do not have measured $T_e(\text{O III})$, we assumed an electron temperature 20% lower than $T_e(\text{N II})$ for the double ionized ions. Since the abundance estimates are barely dependent on the assumed electron density, we adopted for all ionic zones fixed densities of 750 and 440 cm^{-3} (the $[\text{S II}]$ densities from the integrated spectra) for NGC 2579 and ESO 370-9, respectively. Ionic metal abundances were obtained with the *ionic* routine of the *nebular* package of the *STSDAS/IRAF*. The references for atomic parameters used are listed in Table 2 of Krabbe & Copetti (2006). The ionic helium abundances were derived from the strongest lines $\lambda 4471$, $\lambda 5876$, and $\lambda 6678$, using the He I emissivities of Benjamin et al. (1999), which are corrected by the effects of collisional excitation.

The total abundance is the sum of all measured ionic abundances of a given element corrected for unseen ionization stages. We have followed an ionization correction scheme adapted from that of Liu et al. (2000) for Cl, and of Kingsburgh & Barlow (1994) for the other elements based on the similarities between the ionization potentials of different ions and on photoionization models. No precise abundance measurement of neutral elements was possible for NGC 2579. The detected lines of $[\text{N I}]$ were very weak and the $[\text{O I}]$ lines were heavily contaminated by telluric emission. Assuming that the fraction of any neutral heavy elements X^0/X is the same as that of neutral hydrogen H^0/H , which is an adequate assumption according to Kingsburgh & Barlow (1994), especially for the elements O and N, we can ignore the abundances of all neutral species, since in this case we have, as a very good approximation,

$$X/H \approx \sum_{i=1}^{\infty} X^{i+}/H^+ \quad (1)$$

Based on the spectral types of the ionizing stars of NGC 2579 (see Sect. 5), we do not expect a significant amount of neutral gas inside the nebula. We have verified that the helium lines present uniform intensities relative to $\text{H}\beta$ across the nebula, indicating that this element is fully ionized, as expected. This is not the case of ESO 370-9, which is a low ionization nebula. On the

Table 6. Ionic and total abundances (in the scale $12 + \log(X/H)$)

λ_0	Abund.	NGC 2579	ESO 370-9	Orion
4471	He ⁺ /H ⁺	10.93 ± 0.01	10.83 ± 0.06	
5876	He ⁺ /H ⁺	11.02 ± 0.02	10.77 ± 0.03	
6678	He ⁺ /H ⁺	10.94 ± 0.01	10.83 ± 0.02	
avg.	He ⁺ /H ⁺	10.96 ± 0.04	10.81 ± 0.02	
	He/H	10.96 ± 0.04	11.14 ± 0.18	10.99
3727	O ⁺ /H ⁺	7.65 ± 0.16		
4959	O ⁺⁺ /H ⁺	8.32 ± 0.06	7.75 ± 0.11	
5007	O ⁺⁺ /H ⁺	8.30 ± 0.05	7.73 ± 0.11	
avg.	O ⁺⁺ /H ⁺	8.31 ± 0.06	7.73 ± 0.11	
	O/H	8.39 ± 0.05	8.33 ± 0.20	8.47
5518	Cl ⁺⁺ /H ⁺	5.02 ± 0.05		
5538	Cl ⁺⁺ /H ⁺	5.04 ± 0.05		
avg.	Cl ⁺⁺ /H ⁺	5.03 ± 0.05		
	Cl/H	5.16 ± 0.08		5.16
3869	Ne ⁺⁺ /H ⁺	7.60 ± 0.08		
3968	Ne ⁺⁺ /H ⁺	7.54 ± 0.11		
avg.	Ne ⁺⁺ /H ⁺	7.59 ± 0.08		
	Ne/H	7.68 ± 0.06		7.71
6548	N ⁺ /H ⁺	6.61 ± 0.12	7.24 ± 0.10	
6584	N ⁺ /H ⁺	6.63 ± 0.12	7.21 ± 0.08	
avg.	N ⁺ /H ⁺	6.63 ± 0.12	7.22 ± 0.09	
	N/H	7.37 ± 0.06	7.35 ± 0.12	7.62
4069	S ⁺ /H ⁺	5.18 ± 0.12		
6716	S ⁺ /H ⁺	5.31 ± 0.13	5.93 ± 0.08	
6731	S ⁺ /H ⁺	5.31 ± 0.12	5.93 ± 0.08	
avg.	S ⁺ /H ⁺	5.30 ± 0.12	5.93 ± 0.08	
6312	S ⁺⁺ /H ⁺	6.78 ± 0.08		
	S/H	6.91 ± 0.11	6.75 ± 0.19	6.97
7136	Ar ⁺⁺ /H ⁺		6.05 ± 0.08	
	Ar/H		6.43 ± 0.19	6.52

other hand, we have not detected any high excitation emission line, as the He II and $[\text{Ar IV}]$ lines, implying that triple ionized ions are not present in significant quantities. These and other similar arguments justify the following expressions adopted for calculating the total abundances:

$$\text{O}/\text{H} = \text{O}^+/\text{H}^+ + \text{O}^{++}/\text{H}^+, \quad (2)$$

$$\text{N}/\text{H} = (1 + \text{O}^{++}/\text{O}^+) \times \text{N}^+/\text{H}^+, \quad (3)$$

$$\text{Ne}/\text{H} = (1 + \text{O}^+/\text{O}^{++}) \times \text{Ne}^{++}/\text{H}^+, \quad (4)$$

$$\text{Ar}/\text{H} = 1.87 \times \text{Ar}^{++}/\text{H}^+, \quad (5)$$

$$\text{S}/\text{H} = (1 - (1 + \text{O}^+/\text{O}^{++})^{-3})^{-1/3} \times (\text{S}^+/\text{H}^+ + \text{S}^{++}/\text{H}^+), \quad (6)$$

$$\text{Cl}/\text{H} = (\text{S}/\text{H})/(\text{S}^{++}/\text{H}^+) \times \text{Cl}^{++}/\text{H}^+. \quad (7)$$

To derive the total abundances of ESO 370-9, in the absence of measurements of $[\text{O II}]$ and $[\text{S III}]$ lines, we have relied upon the abundance ratios $\text{He}^+/\text{He} = 46.1\%$, $\text{O}^{++}/\text{O} = 24.9\%$, $\text{Ar}^{++}/\text{Ar} = 41.6\%$, and $\text{S}^+/\text{S} = 15.3\%$, obtained by fitting the intensities of the strong emission lines with the photoionization code Cloudy (Ferland et al., 1998).

Table 6 presents the ionic abundances obtained from different lines, the weighted-by-the-line-intensity average values, and the total abundances for the sum of the spectra obtained for NGC 2579 at positions A, B, and C, and for ESO 370-9, all expressed in the logarithmic scale $12 + \log(X/H)$. The error estimates for NGC 2579 correspond to the mean absolute deviation of the abundances obtained at these three different positions. For ESO 370-9 the errors in the ionic abundances were obtained by

Table 7. Electron density and radial velocity statistics

	v_{LSR} (km s ⁻¹)		N_e (cm ⁻³)	
	NGC 2579	ESO 379-9	NGC 2579	ESO 379-9
N	298	40	298	40
min	42.22	56.76	<100	133
Q_1	50.00	58.46	225	225
median	53.03	61.33	376	303
Q_3	57.00	63.91	518	354
max.	68.98	66.82	1886	530
mean	54.70	61.40	435	305
σ	5.28	2.68	491	76

propagation of the errors in the line intensities and electron temperature, while in the case of total abundances, an error of 50% in the ionization correction factors was assumed. For comparison, we also show in this table the total abundances obtained by Esteban et al. (1998) for the Orion Nebula. No temperature fluctuation correction was applied to the total abundances. Although the total abundance estimates for ESO 370-9 required large and uncertain ionization corrections they are quite similar to those of NGC 2579.

4. Electron density and radial velocity maps

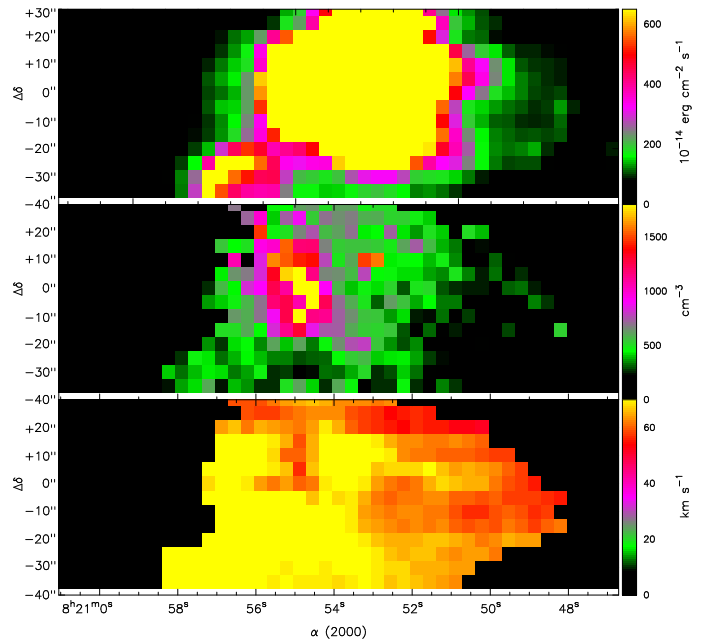
Figure 2 presents the $5'' \times 5''$ resolution maps of $H\alpha$ flux, [S II] electron density and radial velocity with respect to the local standard of rest constructed from the equally spaced long-slit spectroscopic observations. A mask, defined by the positions with $H\alpha$ flux larger than 0.1% of the peak value, was used to delimit the nebula. Only about half of ESO 370-9 was covered by the observations. Table 7 presents some statistics of density and velocity measurements, including the number N of distinct nebular areas, the median, the first and third quartiles, Q_1 and Q_3 respectively (limits between which 50% of the values lie), the minimum and maximum, and the weighted by the $H\alpha$ flux mean and the standard deviation σ .

NGC 2579 and ESO 370-9 sit on a common velocity plateau of $v_{\text{LSR}} \approx 60\text{--}66$ km s⁻¹, indicating that both objects are at a similar distance. From CO observations towards the area, a comparable velocity of $v_{\text{LSR}} = 68.3 \pm 0.3$ km s⁻¹ was obtained by Brand et al. (1987). Parts of NGC 2579, especially in the western and in the northern-central areas, show significantly lower velocities, indicating an internal systematic flow of ionized matter, with the gas streaming away from the main body of the nebula and from the associated molecular cloud with velocities of ≈ 15 km s⁻¹.

As previously indicated by the spatial profile of electron density along a single direction across the nebula (corresponding to offset declination $\Delta\delta = 0$) obtained by Copetti et al. (2000), NGC 2579 presents a non-uniform density structure. The electron density presents steep gradients, especially towards the east, with the density ranging from about 1800 cm⁻³ at the brightest eastern-central areas to less than 100 cm⁻³ at the outer parts of the nebula. Both the velocity and density structures of NGC 2579 suggest that a ‘blister’ (Israel, 1978) or ‘champagne’ (Tenorio-Tagle, 1979) flow is taking place in the nebula.

5. Ionizing stars

Table 8 presents the designations and equatorial coordinates of the five brightest stars towards NGC 2579 and ESO 370-9 which

**Fig. 2.** Maps of the $H\alpha$ flux (upper panel), electron density (mid panel), and LSR radial velocity (lower panel)

were the targets for our spectroscopic and photometric studies for the identification of the ionizing stars of these two nebulae and for the determination of their distances. Hereafter we will designate these stars by their entry numbers in this table.

5.1. Spectral classification

Star 1, which is the brightest star, was the only one with a previous spectral classification. We confirm the spectral type of K1 III attributed for this star by Herbst (1975). For the spectra of stars 2, 3 and 4 embedded in bright parts of NGC 2579 the background subtraction to eliminate nebular emission lines was difficult, so a spectral classification based solely on Balmer or He I lines would be unreliable. Fortunately, these stars show relatively strong He II absorption lines, which could not possibly be a fake result of the background subtraction. So, from a visual inspection the spectral atlas of O stars by Walborn & Fitzpatrick (1990) and especially from the comparison of the equivalent widths of the He II absorption lines with those from Conti (1973) and Conti & Alschuler (1971) we attribute spectral type of O5 V, O6.5 V, and O8 V for stars 2, 3, and 4, respectively. For star 5, the central star in ESO 370-9, we found a spectral type of O8.5 V.

5.2. Distance

Table 9 presents the results of the UBV photometry for the five stars studied, together with the spectral type Sp and some physical properties derived from the spectral classification, namely the visual absolute magnitude M_V for O stars taken from Vacca et al. (1996), the intrinsic color $(B - V)_0$ (and M_V for the K1 III star) from Schmidt-Kaler (1982), and the Lyman continuum photon flux $Q(H^0)$ from Schaerer & de Koter (1997). Also shown in this table are the color excess $E(B - V) = (B - V) - (B - V)_0$ and the heliocentric distance D calculated assuming a visual reddening of $A_V = 3.1E(B - V)$. It is clear from this table that star 1 is a cold foreground star. The others, including star 5 in ESO 370-9, are hot O type stars with comparable reddening and distance es-

timates. Thus, we conclude that NGC 2579 and ESO 370-9 are at a similar heliocentric distance of 7.6 kpc. The dispersion among the distance estimates for these four stars is only 2%, and the propagated photometric error is quite small. However, the photometric distance is strongly dependent on the assumed properties of the stars, especially the value of M_V . The adoption of the absolute visual magnitudes for O stars from Schmidt-Kaler (1982) would result in 13% higher distances, while based on the recent calibration of Martins et al. (2005) we would obtain distances 12% lower. On the other hand, the use of $(B - V)_0$ from other sources, for example from Fitzgerald (1970), would produce distances only 1–2% different. Thus, taking into account the uncertainties in the intrinsic stellar properties adopted, we estimate an error for the photometric distance of about 0.9 kpc

Brand & Blitz (1993) found for the object BBW 138 (\equiv Bran 138), positively identified with NGC 2579, a photometric distance of 11.43 ± 2.33 kpc, which is 50% higher than our distance estimate. They used the Walraven photometric system (*VBLUW*) to derive the distance, as described in Brand & Wouterloot (1988), but the specific photometric data for NGC 2579 has not been published (as far as we know). Therefore, we refrain from making deeper comparison between our results.

The radial velocity map (Fig. 2) clearly indicates that NGC 2579 and ESO 370-9 are at a similar distance. From the measurements of the radial velocity $v_{\text{LSR}}(\text{CO}) = 68.3 \pm 0.3$ km s^{-1} , from CO observations obtained by Brand et al. (1987) (for BBW 138), $v_{\text{LSR}}(5 \text{ GHz}) = 64$ km s^{-1} , from radio recombination lines H 109 α and H 110 α by Caswell & Haynes (1987) (for the object refereed by $254.676 + 0.229$), and $v_{\text{LSR}}(\text{H}\alpha) = 63$ km s^{-1} , the mean velocity of the velocity plateau from the present papers (see Sect. 4), we have calculated a kinematic distance of 7.4 ± 1.4 kpc for NGC 2579 by means of the rotation curve for the Galaxy from Brand & Blitz (1993) assuming the solar galactocentric distance $R_\odot = 8.5$ kpc and velocity $\Theta_\odot = 220$ km s^{-1} . This kinematic distance is entirely compatible with the photometric distance estimated by us.

The distance of the nebula can also be estimated from the observed fluxes in Balmer lines assuming no leakage of ionizing photons from

$$D = \sqrt{\frac{h\nu_{\text{H}\beta} \alpha_{\text{H}\beta}^{\text{eff}}(\text{H}^0, T_e) Q(\text{H}^0)}{4\pi \alpha_{\text{B}}(\text{H}^0, T_e) F(\text{H}\beta) 10^{c(\text{H}\beta)}}}, \quad (8)$$

where $h\nu_{\text{H}\beta}$ is the energy of the H β photon, $\alpha_{\text{H}\beta}^{\text{eff}}(\text{H}^0, T_e)$ is the effective recombination coefficient for H β and $\alpha_{\text{B}}(\text{H}^0, T_e)$ is the total recombination coefficient to excited levels of H. Comparing the integrated H α flux obtained in this paper (see Sect. 2.3) with the H β flux of $\log F(\text{H}\beta) = -10.72$ (in units of erg $\text{cm}^{-2} \text{s}^{-1}$) from Copetti (2000), we calculate a global extinction of $c(\text{H}\beta) = 1.91$ (from the stellar photometry we get $c(\text{H}\beta) = 1.5E(B - V) = 1.96$, and from the spectroscopy at selected positions $c(\text{H}\beta) \approx 1.6$). The total rate of ionizing photons $Q(\text{H}^0)$ was obtained adding together the values shown in Table 9 for individual stars. Although we have to make strong assumptions in this method, we obtained a comparable distance of 10.5 kpc, only 40% higher than the photometric distance. This distance estimate is also strongly dependent on the adopted parameters for O stars, and the uncertainties on $Q(\text{H}^0)$ are high. For example, based on the models of Martins et al. (2005) we would derive about half of the ionizing photon flux obtained from the calibration with the spectral type by Schaerer & de Koter (1997). More importantly, inverting the arguments, we can show that, assuming the photometric distance obtained for the pair NGC 2579

and ESO 370-9, stars 2, 3, 4, and 5 may be solely responsible for the required budget of ionizing photons. For a distance of 7.6 kpc (and $c(\text{H}\beta) = 1.91$), from the observed H α fluxes we derive $\log Q(\text{H}^0) = 49.40$ for NGC 2579 and $\log Q(\text{H}^0) = 48.46$ for ESO 370-9 (in units of s^{-1}), while from the spectral types we estimate $\log Q(\text{H}^0) = 49.71$ and 48.64, respectively. These figures may be considered compatible, since errors of the order of 0.30 dex are expected for $Q(\text{H}^0)$.

6. Discussion

NGC 2579 is an interesting object not only due to its high surface brightness but especially because of its location in the Galaxy. The estimated heliocentric distance of $D = 7.6$ kpc corresponds to a galactocentric distance of $R = 12.8$ kpc. With a moderate interstellar extinction of about 0.5 magnitudes in *V* per kiloparsec, NGC 2579 may contribute significantly to the studies of the abundance gradients in the outer Galaxy, since it has been very difficult to find in this part of the Galaxy objects bright enough to allow direct abundance determinations (Fich & Silkey, 1991; Vilchez & Esteban, 1996). In fact, NGC 2579 is one of the most distant Galactic H II region for which the emission line ratio $[\text{O III}](\lambda 4959 + \lambda 5007)/\lambda 4363$ has been already measured. The metal abundances measured in NGC 2579 are slightly lower (by 24% in mean and by 20% for the O/H) than those in the Orion Nebula. The helium abundance is lower than in Orion by 7%. From the comparison of the oxygen abundances of these two nebulae alone we would derive a shallow abundance gradient of -0.02 ± 0.01 dex/kpc for the galactocentric distance range $8.8 < R$ (kpc) < 12.8 . A more complete investigation of the impact of the chemical composition determination of NGC 2579 on the abundance gradients in the Galaxy will be present elsewhere.

6.1. The nature of ESO 370-9

ESO 370-9 is a roughly elliptical $40'' \times 50''$ ringed nebula with a star in the middle. Because of this morphology it has been misclassified as a planetary nebula. With a mean linear diameter of ≈ 1.6 pc it is comparable in size with the largest planetary nebulae. However, ESO 370-9 is definitively too massive to be a planetary nebula. Assuming an electron density of $N_e = 440 \text{ cm}^{-3}$ (the integrated $[\text{S II}]$ density from Table 5), an electron temperature of $T_e = 10^4$ K, a Lyman continuum photon flux of $\log Q(\text{H}^0) = 48.46$ (in units of s^{-1}), an ionized helium abundance of $y^+ = 0.05$ and a total helium abundance of $y = 0.1$, we estimate a mass of $M \approx 28 M_\odot$ using the expression

$$M = \frac{m_p(1 + 4y)}{(1 + y^+) \alpha_{\text{B}}(\text{H}^0, T_e)} \frac{Q(\text{H}^0)}{N_e}, \quad (9)$$

where m_p is the proton mass. Besides, the chemical abundances of ESO 370-9, especially the relative abundance of nitrogen to oxygen of $\text{N/O} \approx 0.10$, are more typical of H II regions. Planetary nebulae usually present higher N/O abundance ratios, on average by a factor of 5 and in extreme cases by a factor larger than 10 (Peimbert & Torres-Peimbert, 1971; Kingsburgh & Barlow, 1994; Perinotto et al., 2004). So, we conclude that ESO 370-9 is a small and relatively low excitation H II region ionized by a single O8.5 V star located at a distance similar to that of NGC 2579 (≈ 7.6 kpc), which leaves the possibility that these two objects are physically associated.

7. Conclusions

We have presented the first comprehensive optical observational study on the nebular and stellar properties of the Galactic H II regions NGC 2579 and ESO 370-9, which includes the determination of electron temperature and density, chemical composition, and the study of the density and radial velocity structures of the nebulae. We have also pursued the identification and spectral classification of the ionizing stars, and the determination of their distances. The nature of ESO 370-9, usually misclassified as planetary or reflection nebula, is discussed. The main conclusions are:

1. The chemical abundances of He, N, O, Ne, S, and Cl measured in NGC 2579 are slightly lower than those in the Orion Nebula, the metal abundances by about 24% on average and the helium abundance by 7%, which is consistent with the chemical composition gradient in the Galaxy.
2. NGC 2579 is ionized by three O stars of spectral types O5 V, O6.5 V, and O8 V, while ESO 370-9 is ionized by a single O8.5 V star. These stars are entirely capable of being solely responsible for the required ionizing photon fluxes estimated from Balmer recombination lines, although other cooler stars should be present.
3. NGC 2579 and ESO 370-9 are at a similar distance. We have estimated from spectroscopic parallax a heliocentric distance of 7.6 ± 0.9 kpc for both objects, which corresponds to a galactocentric distance of 12.8 ± 0.7 kpc (for $R_{\odot} = 8.5$ kpc). A similar kinematic distance of 7.4 ± 1.4 kpc was derived from the H α velocity field.
4. NGC 2579 presents a steep density gradient, with the electron density ranging from about 1800 cm^{-3} at the brightest eastern-central areas to less than 100 cm^{-3} at the outer parts. Both the velocity and density structures of NGC 2579 suggest that a ‘blister’ or ‘champagne’ flow is taking place in the nebula.
5. The estimated mass of gas of $\approx 28 M_{\odot}$ for ESO 370-9 indicates that it can not be a planetary nebula. With a diameter of ≈ 1.6 pc, ESO 370-9 is a small and relatively low excitation H II region ionized by a single O8.5 V star. It is located at about the same distance as NGC 2579.
6. The Galactic H II region NGC 2579 has been neglected for a long time due to identification problems which persisted until recently. It has been misclassified as planetary or reflection nebula and confused with other objects. Because of its high surface brightness, angular size of few arcminutes and relatively low interstellar extinction, it is an ideal object for investigations in the optical range. Besides this, its location at the outer Galaxy and its high excitation make NGC 2579 an essential object for the studies of the Galactic chemical abundance gradients.

Acknowledgements. This work was partially supported by the Brazilian institutions CAPES, CNPq and FAPERGS. We thank the referee, Manuel Peimbert, for helpful comments and suggestions.

References

Acker, A., Marcout, J., Ochsenbein, F., Stenholm, B., & Tylenda, R. 1992, Garching: European Southern Observatory, 1992,
 Archinal, B. A., & Hynes, S. J. 2003, *Star clusters*, Willmann-Bell, 2003.,
 Benjamin, R. A., Skillman, E. D., & Smits, D. P. 1999, *ApJ*, 514, 307
 Brand, J., Blitz, L., & Wouterloot, J. G. A. 1986, *A&AS*, 65, 537
 Brand, J., Blitz, L., Wouterloot, J. G. A., & Kerr, F. J. 1987, *A&AS*, 68, 1
 Brand, J., & Blitz, L. 1993, *A&A*, 275, 67
 Brand, J., & Wouterloot, J. G. A. 1988, *A&AS*, 75, 117
 Caswell, J. L., & Haynes, R. F. 1987, *A&A*, 171, 261

Conti, P. S. 1973, *ApJ*, 179, 161
 Conti, P. S., & Alschuler, W. R. 1971, *ApJ*, 170, 325
 Copetti, M. V. F. 2000, *A&AS*, 147, 93
 Copetti, M. V. F., & Dottori, H. A. 1989, *A&AS*, 77, 327
 Copetti, M. V. F., Mallmann, J. A. H., Schmidt, A. A., & Castañeda, H. O. 2000, *A&A*, 357, 621
 Dreyer, J. L. E. 1888, *New General Catalogue*, Royal Astron. Soc., London
 Esteban, C., Peimbert, M., Torres-Peimbert, S., & Escalante, V. 1998, *MNRAS*, 295, 401
 Ferland, G. J., Korista, K. T., Verner, D. A., Ferguson, J. W., Kingdon, J. B., & Verner, E. M. 1998, *PASP*, 110, 761
 Fich, M., & Silkey, M. 1991, *ApJ*, 366, 107
 Fitzgerald, M. P. 1970, *A&A*, 4, 234
 Galadí-Enríquez, D., Trullols, E., & Jordi, C. 2000, *A&AS*, 146, 169
 Gum, C. S. 1955, *MmRAS*, 67, 155
 Herbst, W. 1975, *AJ*, 80, 212
 Israel, F. P. 1978, *A&A*, 70, 769
 Kaler, J. B. 1976, *ApJS*, 31,
 Kimeswenger, S. 2001, *Rev. Mex. Astron. Astrof.*, 37, 115
 Kingsburgh, R. L., & Barlow, M. J. 1994, *MNRAS*, 271, 257
 Krabbe, A. C., & Copetti, M. V. F. 2005, *A&A*, 443, 981
 Krabbe, A. C., & Copetti, M. V. F. 2006, *A&A*, 450, 159
 Landolt, A. U. 1992, *AJ*, 104, 340
 Lauberts, A., Holmberg, E. B., Schuster, H.-E., & West, R. M. 1981, *A&AS*, 43, 307
 Lindoff, U. 1968, *Arkiv for Astronomi*, 5, 63
 Liu, X.-W., Storey, P. J., Barlow, M. J., Danziger, I. J., Cohen, M., & Bryce, M. 2000, *MNRAS*, 312, 585
 Martins, F., Schaerer, D., & Hillier, D. J. 2005, *A&A*, 436, 1049
 Nordstrom, B. 1975, *A&AS*, 21, 193
 Peimbert, M., & Torres-Peimbert, S. 1971, *ApJ*, 168, 413
 Perinotto, M., Morbidelli, L., & Scatarzi, A. 2004, *MNRAS*, 349, 793
 Rousseau, J. M., & Perie, J. P. 1996, *A&AS*, 115, 517
 Schmidt-Kaler, T. 1982, in *Landolt-Börnstein, New Series, Group VI, Vol.2*, ed. K. Schaifers & H. H. Voigt (Berlin: Springer-Verlag)
 Schaerer, D., & de Koter, A. 1997, *A&A*, 322, 598
 Storey, P. J., & Hummer, D. G. 1995, *MNRAS*, 272, 41
 Tenorio-Tagle, G. 1979, *A&A*, 71, 59
 Vacca, W. D., Garmany, C. D., & Shull, J. M. 1996, *ApJ*, 460, 914
 van den Bergh, S., & Herbst, W. 1975, *AJ*, 80, 208
 Vilchez, J. M., & Esteban, C. 1996, *MNRAS*, 280, 720
 Walborn, N. R., & Fitzpatrick, E. L. 1990, *PASP*, 102, 379

List of Objects

‘NGC 2579’ on page 1
 ‘NGC 2580’ on page 1
 ‘AH03 J0822-36’ on page 1
 ‘RCW 20’ on page 1
 ‘Gum 11’ on page 1
 ‘BBW 138’ on page 1
 ‘VdBH 13a’ on page 1
 ‘VdBH 13b’ on page 1
 ‘VdBH 13c’ on page 1
 ‘NGC 2580’ on page 2
 ‘Ns 238’ on page 2
 ‘ESO 370-9’ on page 2
 ‘NGC 2579’ on page 7

Table 4. Observed and reddening-corrected emission line intensities, $F(\lambda)$ and $I(\lambda)$, respectively (normalized to $H\beta = 100$). Positions A, B and C correspond to $\Delta\delta = 0''$, $8''$ N, and $7''$ S, respectively. The spectrum of ESO 370-9 was obtained at $\Delta\delta = 44''$ S

λ_0 (Å)	Ion	NGC 2579, A			NGC 2579, B			NGC 2579, C			NGC 2579, ABC			ESO 370-9		
		$F(\lambda)$	$I(\lambda)$	error	$F(\lambda)$	$I(\lambda)$	error	$F(\lambda)$	$I(\lambda)$	error	$F(\lambda)$	$I(\lambda)$	error	$F(\lambda)$	$I(\lambda)$	error
3726.03	[O II] }	60.20	159.30	6	79.44	171.20	6	76.76	143.70	6	68.29	156.00	5	—	—	—
3728.82	[O II] }															
3750.15	H I	1.48	3.83	13	1.43	3.03	13	2.23	4.12	14	1.65	3.70	9	—	—	—
3770.63	H I	1.69	4.29	11	2.22	4.63	10	2.07	3.77	11	1.81	3.99	12	—	—	—
3797.90	H I	2.19	5.43	9	2.73	5.58	8	3.57	6.40	9	2.61	5.64	7	—	—	—
3835.39	H I	2.94	7.04	7	3.67	7.30	5	4.16	7.30	5	3.46	7.25	4	—	—	—
3869.06	[Ne III]	10.12	23.48	6	10.95	21.26	6	13.29	22.85	6	11.09	22.65	6	—	—	—
3888.65	He I }	8.54	19.46	5	10.37	19.85	5	11.55	19.63	5	9.66	19.43	5	—	—	—
3889.05	H I }															
3967.79	[Ne III] }	10.86	23.04	4	13.42	24.28	3	15.50	25.16	3	12.75	24.13	3	—	—	—
3970.07	H I }															
4026.19	He I	0.80	1.61	13	1.09	1.89	13	1.49	2.34	9	1.14	2.06	8	—	—	—
4068.60	[S II]	0.31	0.60	25	0.34	0.57	46	0.74	1.13	14	0.41	0.72	22	—	—	—
4101.74	H I	13.43	25.31	5	15.74	25.94	4	17.35	26.09	4	15.06	25.78	3	12.78	25.28	9
4267.26	C II	0.20	0.33	24	0.35	0.52	21	0.37	0.51	24	0.28	0.43	17	—	—	—
4319.63	O II															
4340.47	H I	30.83	47.57	6	33.19	46.72	6	35.21	46.56	6	32.50	46.95	6	29.78	47.50	5
4363.21	[O III]	1.41	2.14	7	1.30	1.80	6	1.12	1.46	7	1.20	1.71	5	—	—	—
4387.93	He I	0.36	0.53	12	0.42	0.57	18	0.64	0.83	8	0.44	0.62	12	—	—	—
4471.48	He I	3.19	4.42	6	3.42	4.43	4	3.29	4.06	4	3.22	4.30	3	2.36	3.35	14
4658.05	[Fe III] }	0.35	0.41	30	0.51	0.58	20	0.30	0.33	19	0.42	0.48	18	—	—	—
4661.63	O II }															
4713.14	He I	0.57	0.64	26	0.34	0.37	20	0.48	0.52	14	0.48	0.53	12	—	—	—
4861.33	H I	100.00	100.00	3	100.00	100.00	3	100.00	100.00	3	100.00	100.00	3	100.00	100.00	4
4881.00	[Fe III]	0.16	0.16	45	0.39	0.38	45	0.23	0.23	50	0.20	0.20	50	—	—	—
4921.93	He I	1.28	1.22	20	1.16	1.11	50	1.25	1.19	20	1.17	1.11	20	—	—	—
4958.91	[O III]	143.30	132.20	4	136.50	126.50	5	139.00	128.20	4	140.50	129.80	5	33.74	31.27	5
5006.84	[O III]	451.50	400.50	5	429.60	383.90	6	437.40	388.10	5	440.80	392.00	5	95.90	85.74	5
5015.68	He I	4.35	3.83	20	3.11	2.76	25	3.15	2.77	15	3.10	2.74	12	—	—	—
5045.10	N II }	0.18	0.15	>50	0.23	0.20	>50	0.29	0.25	40	0.23	0.20	31	—	—	—
5047.74	He I }															
5056.31	Si II	0.16	0.14	>50	0.19	0.16	>50	0.43	0.37	23	0.43	0.37	21	—	—	—
5197.90	[N I] }	0.78	0.59	48	0.44	0.34	42	1.00	0.75	23	0.61	0.46	27	1.13	0.82	12
5200.26	[N I] }															
5270.40	[Fe III]	0.26	0.18	>50	0.44	0.32	44	0.35	0.25	24	0.31	0.22	24	—	—	—
5517.72	[Cl III]	1.13	0.65	13	1.05	0.62	10	1.10	0.63	10	1.12	0.65	10	—	—	—
5537.89	[Cl III]	0.81	0.46	14	0.97	0.57	11	0.84	0.47	16	0.94	0.54	12	—	—	—
5754.64	[N II]	1.03	0.49	10	0.80	0.40	11	1.07	0.51	12	1.00	0.48	10	3.02	1.32	10
5875.59	He I	33.10	14.48	4	30.91	14.23	4	32.91	14.44	4	32.39	14.42	4	20.40	8.11	6
6312.10	[S III]	4.27	1.40	5	4.44	1.56	4	4.51	1.49	4	4.54	1.53	4	—	—	—
6548.04	[N II]	28.96	8.28	5	32.38	10.00	3	30.06	8.64	3	30.80	9.04	3	131.60	32.55	16
6562.80	H I	1008.00	286.00	3	933.30	286.00	3	1004.00	286.00	3	982.90	286.00	3	1167.00	285.80	5
6583.41	[N II]	91.58	25.68	3	106.70	32.35	3	92.16	25.96	3	96.29	27.71	3	364.20	88.07	5
6678.15	He I	12.62	3.36	3	11.74	3.39	4	12.29	3.29	3	11.94	3.35	3	11.10	2.53	5
6716.44	[S II]	17.01	4.44	6	20.40	5.78	4	16.19	4.24	3	18.02	4.83	3	85.55	19.09	8
6730.81	[S II]	17.55	4.54	5	20.88	5.88	3	17.60	4.58	3	18.94	5.04	3	80.11	17.73	10
7065.22	He I	—	—	—	—	—	—	—	—	—	—	—	—	12.03	2.21	5
7135.80	[Ar III]	—	—	—	—	—	—	—	—	—	—	—	—	46.84	8.27	8
c(H β)	H α /H β		1.65			1.55			1.65			1.62			1.84	
c(H β)	H γ /H β , H δ /H β		1.42			1.12			0.91			1.20			1.53	

Table 5. Electron densities and temperatures (in units of cm^{-3} and K, respectively)

	NGC 2579, A	NGC 2579, B	NGC 2579, C	NGC 2579, ABC	ESO 370-9
N_e (S II)	699 ± 219	641 ± 126	869 ± 129	745 ± 114	443 ± 262
N_e (Cl III)	$< 1\,100$	$< 2\,900$	$< 1\,600$	$< 2\,100$	
T_e (N II)	$11\,550 \pm 620$	$9\,630 \pm 430$	$11\,670 \pm 680$	$11\,030 \pm 520$	$10\,300 \pm 790$
T_e (O III)	$9\,490 \pm 230$	$9\,140 \pm 240$	$8\,620 \pm 190$	$8\,960 \pm 210$	

Table 8. Studied stars

Star designation				Position (J2000)		
N	VdBH [†]	DENIS	Other	α	δ	Nebula
1	13a A	J082052.9-361251	CD-35 4502	08 20 52.92	-36 12 51.1	NGC 2579
2	13a B	J082052.8-361258		08 20 52.83	-36 12 58.0	NGC 2579
3	13b A	J082054.8-361258		08 20 54.86	-36 12 58.9	NGC 2579
4	13b B	J082055.0-361306		08 20 55.05	-36 13 06.0	NGC 2579
5	13c	J082056.9-361342		08 20 56.97	-36 13 42.5	ESO 370-9

†Original designations of VdBH 13a and VdBH 13b broken in two stars by Rousseau & Perie (1996) and in this paper, respectively.

Table 9. *UBV* photometry and properties of the studied stars

Star	V	$U - V$	$B - V$	Sp	M_V	$(B - V)_0$	$E(B - V)$	D (kpc)	$Q(\text{H}^0)$ (s^{-1})
1	10.385 ± 0.008	1.377 ± 0.024	1.553 ± 0.017	K1 III	0.61	1.07	0.48	0.45	
2	13.055 ± 0.015	-0.104 ± 0.036	0.934 ± 0.029	O5 V	-5.33	-0.33	1.26	7.82	49.48
3	13.607 ± 0.012	-0.237 ± 0.036	1.038 ± 0.026	O6.5 V	-4.99	-0.32	1.36	7.54	49.17
4	13.910 ± 0.034	-0.099 ± 0.084	1.028 ± 0.072	O8 V	-4.66	-0.32	1.35	7.56	48.80
5	13.748 ± 0.004	-0.184 ± 0.019	0.958 ± 0.008	O8.5 V	-4.55	-0.31	1.27	7.47	48.64